Electronic Supplementary Information

Stimuli-responsive supramolecular micellar assemblies of cetylpyridinium chloride with cucurbit[5/7]uril

Sharmistha Dutta Choudhury,[a] Nilotpal Barooah,[a] Vinod Kumar Aswal,[b] Haridas Pal,[a] Achikanath C. Bhasikuttan,[a] Jyotirmayee Mohanty*,[a]

[a]*Radiation & Photochemistry Division,* [b]*Solid State Physics Division, Bhabha Atomic Research Centre, Mumbai 400 085, India;*

E-mail: jyotim@barc.gov.in

Note-1

SANS Analysis: In SANS experiments, one measures the coherent differential scattering cross-section per unit volume ($d\Sigma/d\Omega$) as a function of Q. For monodispersed particles, $d\Sigma/d\Omega$ can be expressed as[1]

$$\frac{d\Sigma}{d\Omega}(Q) = nV^2(\rho_p - \rho_s)^2 P(Q)S(Q) + B \qquad \text{(S1)}$$

where n is the number density and V is particle volume. ρ_p and ρ_s are scattering length densities of particles and solvent, respectively. $P(Q)$ is the intraparticle structure factor and depends on the shape and size of the particles. $S(Q)$ is the inter particle structure factor decided by the interaction between particles and is unity for dilute systems. B is a constant term representing incoherent background arising mainly due to hydrogen atoms in the system.

The micelles formed at the critical micelle concentration are spherical. If the solution conditions (e.g. concentration, ionic strength etc.) of the micellar solutions are changed that favors the growth of the micelles, they grow along one of the axial directions of the micelles. The growth of the micelles along other two axial directions is restricted by the maximum length of the surfactant molecule to avoid any energetically unfavorable empty space formation or water penetration inside the micelle.[2] The prolate ellipsoidal shape ($a > b = c$) of the micelles is widely used in the analysis of SANS data because it also represents the other different possible shapes of the micelles such as spherical ($a = b = c$), oblate ellipsoidal ($a < b = c$), rodlike ($a >> b = c$) and disclike ($a << b = c$). For such an ellipsoidal micelle[3]

$$P(Q) = \int_0^1 \left[F(Q,\mu)^2 d\mu\right] \qquad \text{(S2)}$$

$$F(Q,\mu) = \frac{3(\sin x - x\cos x)}{x^3} \qquad \text{(S3)}$$

$$x = Q\left[a^2\mu^2 + b^2(1-\mu^2)\right]^{1/2} \qquad \text{(S4)}$$

where a and b are, respectively, the semi-major and semi-minor axes of the ellipsoidal micelle and μ is the cosine of the angle between the directions of a and the wave vector transfer Q.

In general, micellar solutions of ionic surfactants show a correlation peak in the SANS data. The peak arises because of the corresponding peak in the interparticle structure factor $S(Q)$ and indicates the presence of electrostatic interactions between the micelles. $S(Q)$ specifies the correlation between the centers of different micelles and it is Fourier transform of the radial distribution function *g(r)* for the mass centers of the micelles. In the analysis, $S(Q)$ has been calculated as derived by Hayter and Penfold from the Ornstein-Zernike equation and using the mean spherical approximation.[3] The micelle is assumed to be a rigid equivalent sphere of diameter $\sigma = 2(ab^2)^{1/3}$ interacting through a screened Coulomb potential.

The data have been analyzed by comparing the scattering from theoretical models to the experimental data. The calculated neutron scattering length densities of the different components used are given in the Table below. It is clear that scattering length density of CB5 and CB7 are similar to that of D_2O and hence are not visible in the SANS data carried out in D_2O. Therefore most of the scattering measured is from the CPC micelles. Throughout the data analysis, corrections were also made for instrumental smearing. The modelled scattering profiles were smeared by the appropriate resolution function to compare with the measured data. The fitted parameters in the analysis were optimized by means of nonlinear least-square fitting program. The fitted data are given by the solid lines to the experimental data points.

From the neutron scattering length densities of the different components as given below, it is clear that scattering length density of CB5 and CB7 are similar to that of D_2O and hence are not visible in the SANS data carried out in D_2O. The changes in the scattering data are therefore observed as a result of their influence on the CPC micelles. If the SANS data are carried out in H_2O, the scattering is dominated by the incoherent neutron scattering from the solvent.

The neutron scattering length densities of the different components

Component	Chemical Formula	Scattering Length (cm)	Molecular Volume (Å^3)	Scattering Length Density (cm^{-2})
CPC	$C_{21}H_{38}ClN$	0.681×10^{-12}	590	0.12×10^{10}
CB5	$C_{30}H_{30}N_{20}O_{10}$	33.25×10^{-12}	526	6.32×10^{10}
CB7	$C_{42}H_{42}N_{28}O_{14}$	46.54×10^{-12}	718	6.48×10^{10}
solvent	D_2O	1.92×10^{-12}	30	6.40×10^{10}

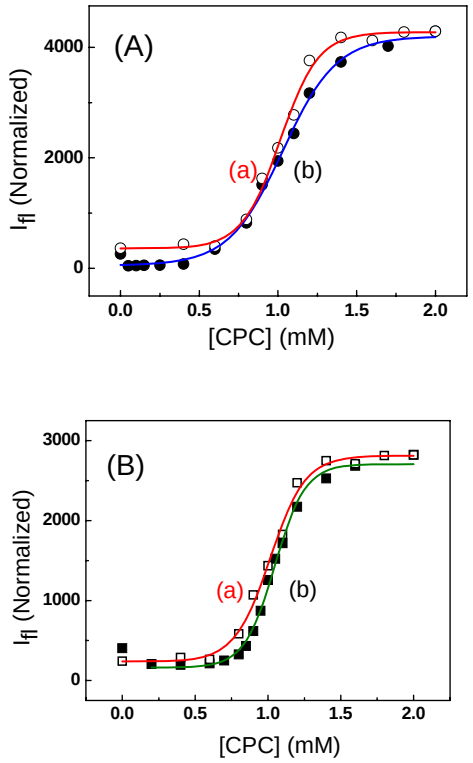

Figure S1. (**A**) Fluorescence titration curves of NR (~2 μM) with CPC in the absence (a) and presence of KCl (2 mM). (**B**) Fluorescence titration curves of NR (~2 μM) with CPC at natural pH (a) and at pH 4 (b). λ_{ex} = 550 nm, λ_{mon} = 660 nm.

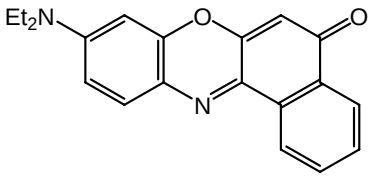

Nile Red (NR)

(Chart S1)

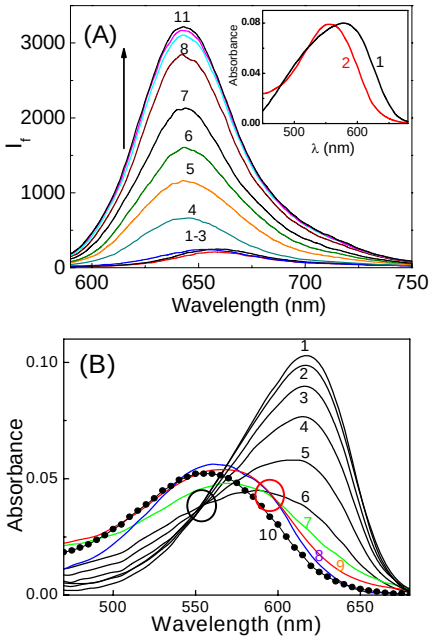

Figure S2. (**A**) Fluorescence spectra of NR (~2 μM) with different concentrations of CPC. [CPC]/mM: 0.0 (1), 0.4 (2), 0.6 (3), 0.8 (4), 0.9 (5), 1.0 (6), 1.1 (7), 1.2 (8), 1.4 (9), 1.8 (10) and 2.0 (11). Inset: Normalized absorption spectra of NR in water (1) and in CPC micelle (2) (**B**) The absorption spectral changes of NR in presence of 2 mM CB7 at different CPC concentrations, [CPC]/mM; 0 (1); 0.9 (2); 1.0 (3); 1.1 (4); 1.2 (5); 1.3 (6); 1.4 (7); 1.7 (8); 2.0 (9). The spectrum (10) indicates the spectrum of NR in CPC micelle. Initially the NR absorption maximum shifts from 578 nm to 618 nm on encapsulation within the CB7 cavity, which gradually reverts to 590 nm on addition of CPC, revealing an isosbestic point at 554 nm. However, at higher concentration of CPC, in addition to a blue shift in the spectral position to ~560 nm, the spectrum became broad, displaying another isosbestic point at 595 nm and becomes almost coincided with the spectral position of NR in the CPC micelle in the absence of CB7 (inset of (A))

Note 2

Interaction of CB7 with Nile Red (NR)

The interaction of NR with CB7 was followed from the changes in the fluorescence intensity of NR. The fluorescence titration and binding curve of NR with CB7 are presented in Fig.S3.

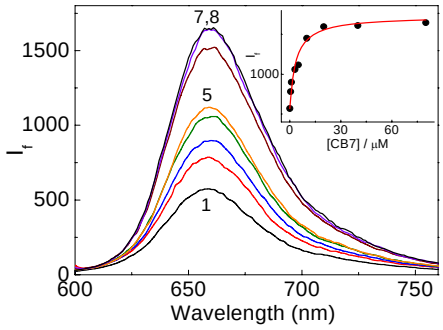

Figure S3. Fluorescence spectra of NR (~2 μM) with different concentrations of CB7. [CB7]/μM: 0 (1), 0.5 (2), 1 (3), 3 (4), 5 (5), 10 (6), 20 (7) and 80 (8). Inset shows the binding isotherm for NR-CB7 complex.

Evaluation of Binding constant of NR-CB7 complex:

The binding constant for CB7-NR complex was evaluated considering 1:1 equilibrium between CB7 host and NR dye, where the observed fluorescence intensity can be expressed as follows[4]

$$I_f = \frac{I_f^0 + I_{CB7.NR} K[CB7]_0}{1 + K[CB7]_0} \quad \text{(S5)}$$

Applying equation (S5), the experimental data were fitted, as shown in the inset of Fig. S3 and the binding constant K thus estimated as $(2.9\pm0.6)\times10^5$ M^{-1}.

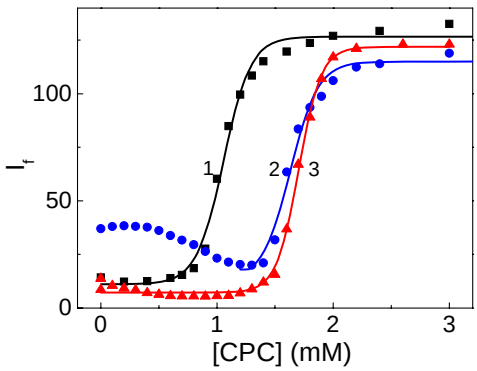

Figure S4. Fluorescence titration curves of NR with different concentrations of CPC in the absence and presence of cyclodextrins (CDs): no CD (1), 1mM β–CD (2) and 1mM α–CD (3), λex = 550 nm, λmon = 660 nm.

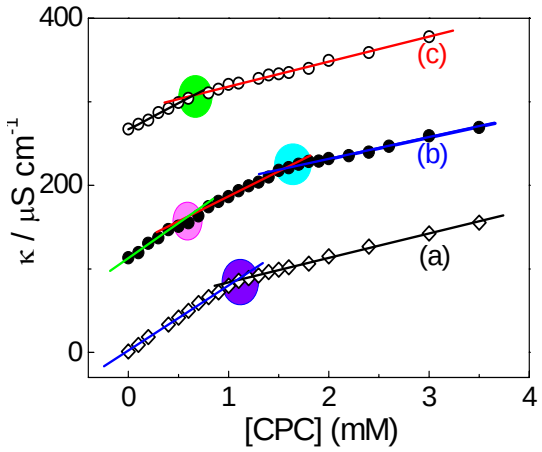

Figure S5: Plots of specific conductance versus CPC concentrations in the absence of CBs (a) and in presence of CB7 (b) and CB5 (c) hosts.

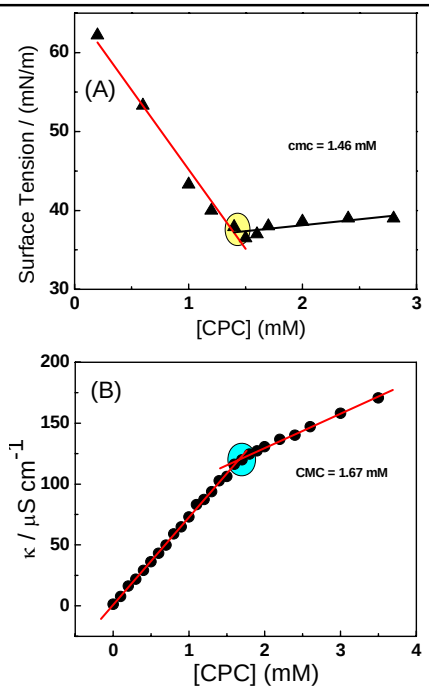

Figure S6: (**A**) Plot of surface tension values versus CPC concentrations in the presence of β-CD (1 mM). (**B**) Plot of specific conductance versus CPC concentrations in the presence of β-CD (1 mM).

Table S1: The *cmc* values obtained for the CPC surfactant, in the absence and presence of macrocyclic hosts, by different experimental methods.

Systems	*cmc* (mM)		
	Fluorescence measurement	Conductivity measurements	Surface tension measurements
CPC	1.0	1.08	0.88
CB7 (1mM)-CPC	1.63[a]	0.57, 1.60	0.65, 1.63
CB5 (1mM)-CPC	0.57	0.60	0.49
βCD (1mM)-CPC	1.67	1.67	1.42

[a] This measurement is carried out in presence of 2mM CB7

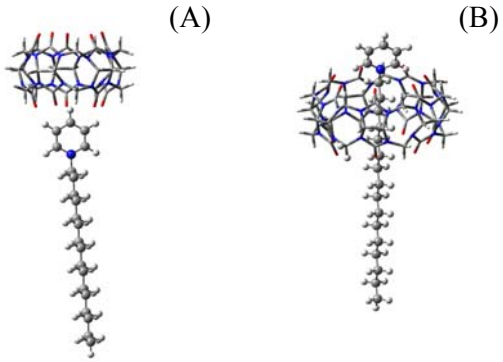

Figure S7. Energy optimized (Gaussian PM3(MM) level) structures of CB5-CPC (A) and CB7-CPC (B) systems.

Note-3

The interaction of CPC with CB7 was followed from the changes in the chemical shift of CPC ^{1}H NMR signal. The shift of the β-CH_2 protons ($\Delta\delta_{obsd}$ at 1.9) at a constant guest concentration $[CPC]_0$ was plotted against the total CB7 concentration $[CB7]_0$. The binding constant value estimated from the nonlinear fitting of the titration curve using equation S6[5] for 1:1 complex was found to be $(2.1\pm0.5)\times10^5$ M^{-1}. The high binding constant value indicates that the complexation certainly involves the ion-dipole interaction between the polar carbonyl portals of CB7 with the pyridyl nitrogen of CPC.

$$\Delta\delta_{obsd} = \left(1 - \frac{[CPC]}{[CPC]_0}\right)\left(\delta_{CB7\bullet CPC} - \delta_{CPC}\right) \qquad \text{(S6)}$$

with

$$[CPC] = \{K[CPC]_0 - K[CB7]_0 - 1 + \sqrt{(K[CPC]_0 + K[CB7]_0 + 1)^2 - 4K^2[CPC]_0[CB7]_0}\}/2K$$

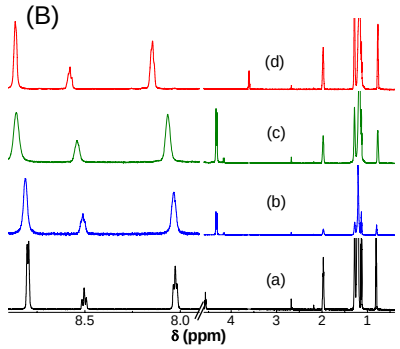

Figure S8. (A) The binding isotherm of CPC (0.5 mM) using NMR titration at different concentrations of CB7. The solid line represents the fitted curve obtained from eq. S6. (B) ^{1}H NMR spectra of CPC (0.3mM) below the *cmc* in the absence (a) and in the presence (b) of 1mM CB5. Spectrum (c) represents the signal of CPC (1mM) above the *cmc* with 1mM CB5. Spectrum (d) represents the signal of CPC (2mM) above the *cmc*.

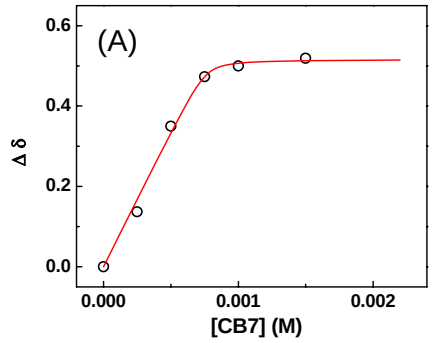

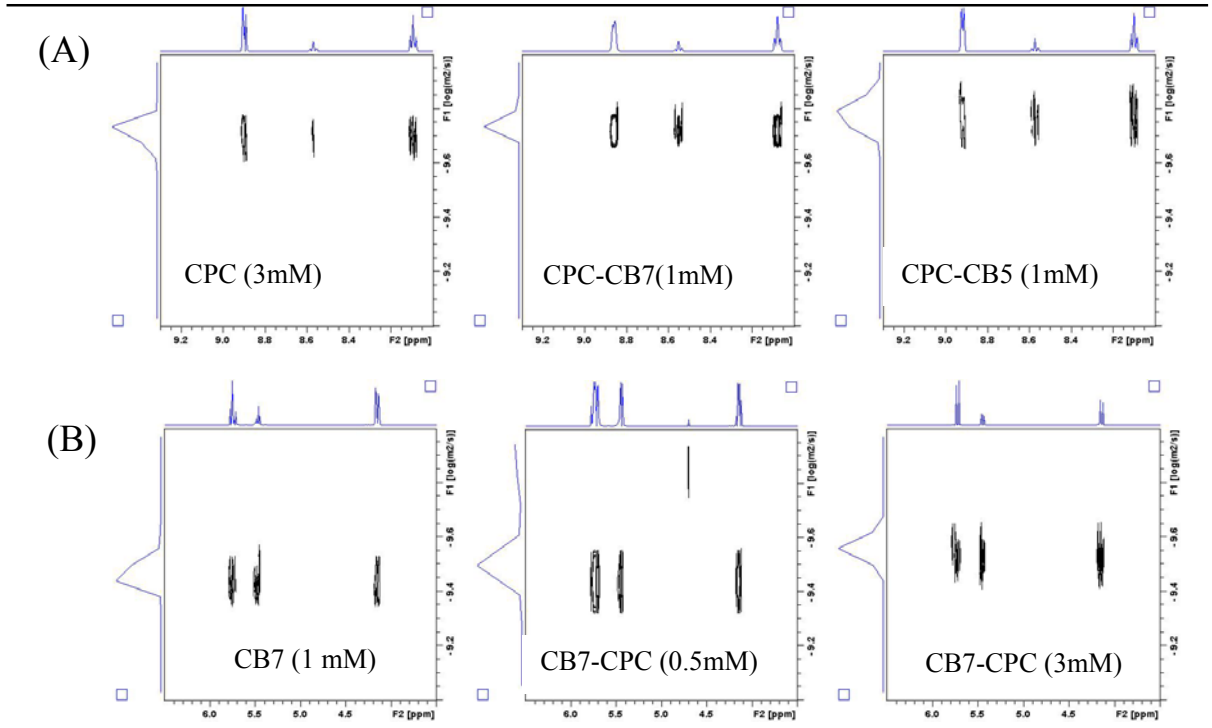

Figure S9. The 1-D and 2-D DOSY spectra of (**A**) CPC (3mM) in the absence and presence of CB7 (1mM) or CB5 (1mM) and (**B**) CB7 (1mM) in the absence and presence of CPC (0.5mM) or CPC (3mM).

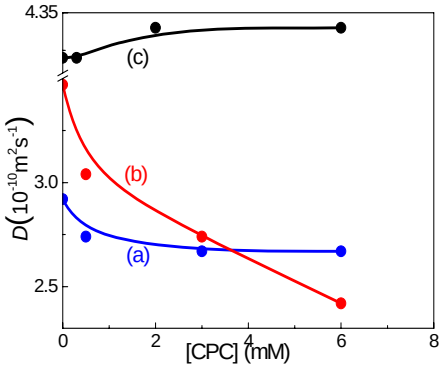

Figure S10: Plot of the diffusion coefficient values for the β-CD (*a*), CB7 (*b*) and the CB5 (*c*) protons with CPC concentration.

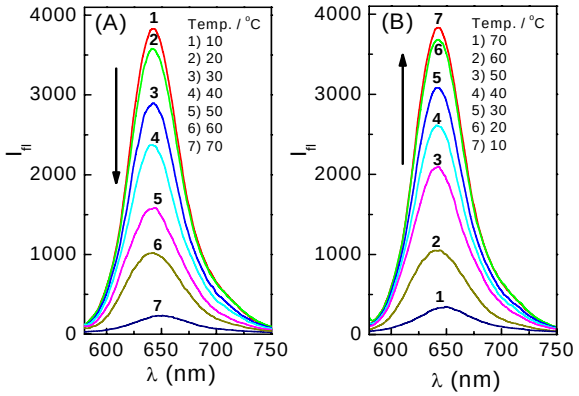

Figure S11: Fluorescence spectral changes in NR-CB5-CPC (0.8 mM) complex with increasing temperature (**A**) and with decreasing temperature (**B**).

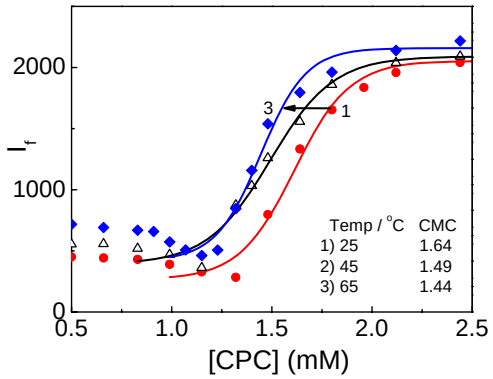

Figure S12: Fluorescence titration curves of NR with different concentrations of CPC in presence of 2mM CB7 at different temperatures. Temp./ºC: 25 (1), 45 (2) and 70 (3). λ_{ex} = 550 nm, λ_{mon} = 660 nm.

1. J.B. Hayter and J. Penfold, *Colloid Polym. Sci.* 1983, **261**, 1022–1030.
2. Y. Chevalier and T. Zemb, *Rep. Prog. Phys.* 1990, **53**, 279–371.
3. J.S. Pedersen, *Adv. Colloid Interface Sci.* 1997, **70**, 171−210.
4. M. K. Singh, H. Pal, A. S. R. Koti,A. V. Sapre, *J. Phys. Chem. A* 2004, ***108***, 1465-1474.
5. W. M. Nau, X. Zhang, *J. Am. Chem. Soc.* 1999, ***121***, 8022-8032.